Polarimetric Calibration of SIR-C Using Point and Distributed Targets

Kamal Sarabandi, *Senior Member, IEEE*, Leland E. Pierce, *Member, IEEE*, M. Craig Dobson, Fawwaz T. Ulaby, *Fellow IEEE*, James M. Stiles, T. C. Chiu, R. De Roo, R. Hartikka, A. Zambetti, and Anthony Freeman, *Senior Member, IEEE*

Abstract— **In preparation for the Shuttle Imaging Radar-C/XSAR (SIR-C/XSAR) flights, the University of Michigan has been involved in the development of calibration procedures and precision calibration devices to quantify the complex radar images with an accuracy of 0.5 dB in magnitude and 5 degrees in phase. In this paper, the preliminary results of the SIR-C calibration and a summary of the University of Michigan's activity in the Raco calibration super-site is presented. In this calibration campaign an array of point calibration targets including trihedral corner reflectors and polarimetric active radar calibrators (PARC's) in addition to a uniform distributed target were used for characterizing the radiometric calibration constant and the distortion parameters of the C-band SAR. Two different calibration methods, one based on the application of point targets and the other based on the application of the distributed target, are used to calibrate the SIR-C data and the results are compared with calibrated images provided by JPL. The distributed target used in this experiment was a field of grass, sometimes covered with snow, whose differential Mueller matrix was measured immediately after the SIR-C overpass using The University of Michigan polarimetric scatterometer systems. The scatterometers were calibrated against a precision metallic sphere and measured 100 independent spatial samples for characterizing the differential Mueller matrix of the distributed target to achieve the desired calibration accuracy. The L-band SAR has not yet been adequately calibrated for inclusion here.**

I. Introduction

In radar remote sensing, calibration of polarimetric radar systems is of great importance because the success of any inversion algorithm or any radar classifier depends directly on the accuracy of the measured data. An external calibration must be performed both to provide a quantitative value for the measured backscatter and to remove the distortion from different channels of the radar, caused by the active components and the antenna. In recent years, calibration of imaging radar systems has been the subject of intensive investigations and many calibration algorithms have been developed [1]–[3], [5], [6]. An excellent review of recent work in SAR calibration can be found in [4]. The external calibration of a radar system involves a comparison of the measured response of the unknown target with the measured response of one or more calibration targets with known radar response. For this purpose, appropriate calibration targets and convenient calibration algorithms are required. In general, existing calibration methods can be categorized into two major groups: 1) calibration techniques based on point calibration targets, and 2) calibration techniques based on distributed calibration targets [7], [8]. Calibration algorithms based on point calibration targets are relatively simple, however, they have been shown to be not very accurate [9]. The inaccuracies using point targets can be attributed to the uncertainties in the SAR-measured RCS of the calibration targets which can be caused by the coherent and incoherent interaction of the background with the calibration targets, errors in orientation of the calibration targets, and the inherent instabilities of the RCS of the calibration targets.

Calibration algorithms based on distributed calibration targets on the other hand are difficult, but their accuracy can be very high [8]. The difficulty of the distributed target calibration method is a result of characterizing the polarimetric response of a relatively large homogeneous distributed target. This task must be accomplished by a calibrated radar system immediately before or after the SAR measurement. In any backscatter measurement of distributed targets the quantities of interest are the backscatter coefficients, which are the second moments of the scattered field per unit area. Calibration algorithms based on point targets for synthetic aperture radars must infer the radiometric calibration constant from the RCS of the point targets. Ideally, this process requires accurate knowledge of the SAR impulse function, which is very difficult to characterize. However, this problem is circumvented in distributed target calibration algorithms where the differential Mueller matrices of a homogeneous target are compared. An approximate technique for dealing with this same issue is described in [5].

As mentioned, accurate calibration of polarimetric imaging radars involves many steps. For the SIR-C calibration project we focused our activities in four areas: 1) development of calibration techniques for the purpose of characterizing the scattering matrices of the calibration targets used in SAR calibration, 2) design and characterization of precision calibration targets appropriate for imaging radars, 3) development of a calibration technique for measurement of differential Mueller matrices of distributed targets which is required both for cross calibration and for calibration methods based on known dis-

Manuscript received December 20, 1994; received March 24, 1995. This work was supported in part by the Jet Propulsion Laboratory, Pasadena, CA, under contract NASA-JPL-958749.

K. Sarabandi, L. Pierce, M. C. Dobson, F. T. Ulaby, J. Stiles, T. C. Chiu, R. De Roo, R. Hartikka, and A. Zambetti are with the Radiation Laboratory, Department of Electrical Engineering and Computer Science, University of Michigan, Ann Arbor, MI 48109-2122, USA.

A. Freeman is with the Jet Propulsion Laboratory, California Institute of Technology, Pasadena, CA 91109 USA.

IEEE Log Number 9412804.

tributed targets, and 4) development of calibration algorithms based on point and distributed targets for imaging radars. Our campaigns for calibration of SIR-C for both the April and the October flights were concentrated at Raco, MI. In this "calibration super-site" both point and distributed calibration targets were employed. An array of point calibration targets including trihedral corner reflectors and PARC's in addition to a uniform distributed target were used for characterizing the radiometric calibration constant and the distortion parameters of the SAR's. In this paper, a summary of the techniques involved in the calibration of SIR-C data and some preliminary results are presented.

II. Preparation for SIR-C Calibration

Over the past five years, in preparation for calibration of SIR-C data many techniques, algorithms, and devices have been developed at the University of Michigan. In this section a brief summary of these accomplishments is given.

A. Calibration Techniques for Point Targets

Three distinct algorithms have been developed for the measurement of scattering matrices of point targets. Our objective in the development of these algorithms was to characterize the scattering matrices of calibration targets used for calibration of SAR's with a high degree of accuracy. The choice of the calibration algorithm depends on the particular system and the accuracy-versus-complexity criterion. For example, in a calibration technique which is referred to as IACT (isolated antenna calibration technique) only a metallic sphere and any other target with relatively high cross-polarized component are required to determine the radar distortion parameters [10]. The scattering matrix of the depolarizing target need not be known. This technique is very convenient, however it is only applicable to radar systems with low cross-talk.

Another calibration technique that is not based on any *a priori* knowledge of the system was also developed [11]. In this technique the transmit and receive distortion matrices of the radar system are characterized using three independent targets with known scattering matrices. Although this method is very general, its drawback is the errors caused by orienting the calibration targets with respect to the antenna system coordinate frame. Using the property of reciprocal passive antennas, a convenient calibration technique was later developed that determines the distortion parameters of a radar system using only a metallic sphere [12]. This technique is referred to as STCT (single target calibration technique). Using this calibration technique the scattering matrix elements of a target can be measured with an accuracy of 0.5 dB in magnitude and ± 5 degrees in phase. STCT was adopted for the measurement of PARC's and trihedrals used in SIR-C calibration. This technique was also used to calibrate the polarimetric scatterometers used in the characterization of the radar response of the distributed calibration target.

B. Measurement of Differential Mueller Matrix of a Distributed Target

The overall accuracy of a calibration procedure for imaging radars can be assessed if an independent accurate measurement of an area within the image were available. With this purpose in mind, we developed an algorithm for backscatter measurement of uniform distributed targets using a scatterometer system. A major difficulty in the Mueller matrix measurement of distributed targets is the lack of known distributed targets, and therefore the calibration coefficient must be inferred from point calibration targets. This process is rather complex, particularly when the radar distortions vary over the illuminated area. This is the case when a scatterometer is used for the measurement. Amplitude and phase variation of the radiation pattern of the scatterometer antenna causes variation in the distortion parameters of the radar over its illuminating area. In this case the distortion parameters must be determined over the entire main beam of the radar system. This is done using a precision metallic sphere in conjunction with STCT in an anechoic chamber. Fig. 1 shows the polarimetric response of the sphere in the azimuth-over-elevation coordinate system (Ψ, ξ) over the mainlobe of our X-band scatterometer system. The distortion parameters of the scatterometer derived from this information is then used to accurately measure the differential Mueller matrix of a distributed target [7]. In practice, accurate characterization of the Mueller matrix using the scatterometer system involves two other steps. While collecting data in the field, the scatterometer should periodically collect backscattering data from the metallic calibration sphere at boresight to monitor the changes in the distortion parameters measured in the anechoic chamber which might be caused by the variations of active components. The measurement is only needed at boresight since the relative variation of the distortion parameters over the main beam is only a feature of the antenna system which is independent of instabilities in the active components of the radar. The final step is postprocessing. All the collected samples must be Fourier transformed and range gated to separate the target response from the other system returns. To keep track of system drift between the calibration sphere measurement and the distributed target measurement, response of a constant system return such as the circulator leakage in the two measurements are compared. That is, the circulator leakage which does not change with time is used as a reference between the two measurements.

Using this procedure, the differential Mueller matrix of an area can be determined, which in turn can be used to calibrate a polarimetric SAR. In such a calibration technique, it can be shown that the impulse response of the SAR (ambiguity function) need not be determined. The detailed procedure and experimental results of the Mueller matrix measurement is given in [7].

C. Characterization and Design of Precision Calibration Targets

There are significant differences between point calibration targets used for conventional (nonimaging) radars and imaging radars. These differences are the direct result of the target deployment configuration. For imaging radars, the calibration targets are placed on the ground (in the presence of a distributed target), whereas in the case of conventional radars the calibration targets are placed in free space. The success

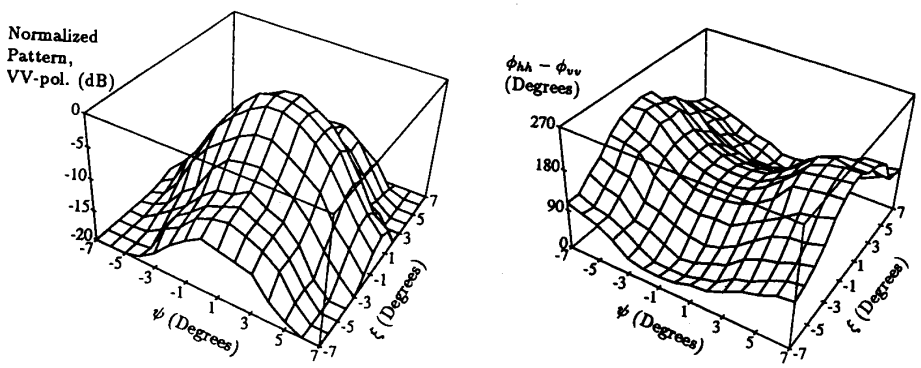

Fig. 1. Backscatter response of a metallic sphere over the main lobe of X-band scatterometer which corresponds to the amplitude and phase variation of the distortion parameters. (The azimuth direction is Ψ, and the elevation direction is ξ.)

of an external calibration procedure is directly influenced by five characteristics of the calibration target. These include 1) large radar cross section (RCS), 2) wide RCS pattern, 3) small physical size, 4) stable RCS, and 5) insensitivity of RCS to the surrounding environment. Noting that the calibration targets are deployed over a surface with a nonzero radar backscatter, it is required that the RCS of the target be much larger than the direct backscatter of the terrain and also the coherent interaction of the target and the terrain be as small as possible. The wide RCS pattern or insensitivity of target alignment to the radar coordinate and the small physical size requirements are needed to assure the ease of target deployment under field conditions.

Calibration targets, in general, can be categorized into two major groups: 1) passive and 2) active [5]. Passive calibrators are more stable and reliable than their active counterparts, however, their large physical size is their major drawback. Trihedral corner reflectors are the most widely used targets for imaging radars because of their high RCS and wide RCS pattern. Eight-foot trihedral corner reflectors were chosen as point targets for SIR-C calibration. These trihedrals were designed at JPL and are comprised of three detachable panels. Each panel is made up of a thin perforated aluminum sheet attached over a triangular frame. Due to light structural design of these panels the trihedrals can experience some geometrical deformation during field deployment. Geometrical deformation of trihedrals can significantly affect their expected RCS [14]. Fig. 2 shows the measured and calculated (geometrical optics) RCS pattern of a typical 8-foot trihedral at L-band. To characterize the uncertainty in RCS of the trihedral, the RCS measurements were repeated many times, each time after dismantling and reassembling the trihedral. It was found that the uncertainty in the RCS of the trihedrals at L-band is about ± 1.5 dB.

In recent years, polarimetric active radar calibrators (PARC's) have been used extensively. In addition to high RCS and wide RCS pattern, PARC's are desirable for their relatively small physical size. In the standard design, PARC's are comprised of two antennas: one used as the receiver and the other used as the transmitter. In the RCS characterization of such PARC's, it was found that the RCS patterns were nonsymmetric and the phase patterns exhibited

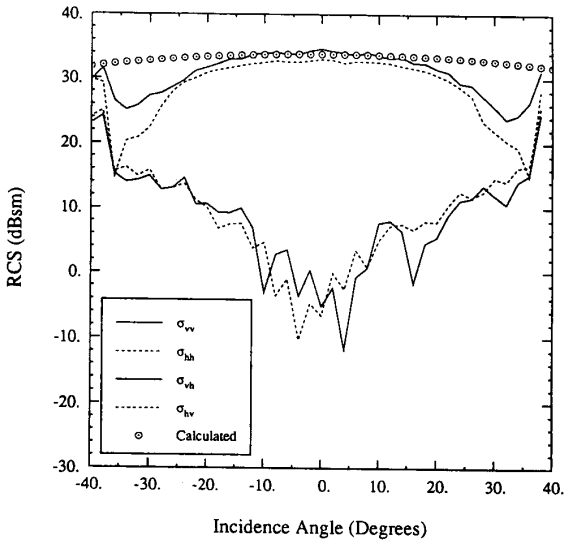

Fig. 2. A typical measured L-band RCS of an 8-foot trihedral in the azimuth plane.

rapid fluctuations which were caused by close proximity of the transmit and receive antennas [15]. These undesirable characteristics prompted design of a novel single antenna PARC. The new PARC can provide a very high RCS while having a relatively small physical size [16]. L-band and C-band single antenna PARC's (SAPARC's) were designed and deployed as point calibration targets during the SIR-C experiments. Each SAPARC is a dual-polarized antenna in conjunction with an ortho-mode transducer (OMT) with isolation of 40 dB. One branch of the OMT is used as the transmitter while the other is used as the receiver. Fig. 3 shows the simplified block diagram of the L-band SAPARC. Figs. 4 and 5 show the RCS patterns of the L- and C-band SAPARC's, respectively, when the antenna ia rotated 45° with respect to the incident polarization. The variation of the RCS of the SAPARC's versus temperature was characterized very carefully. The SAPARC's are equipped with a temperature recorder device to record the system's temperature accurately during the SIR-C measurements. The recorded temperature

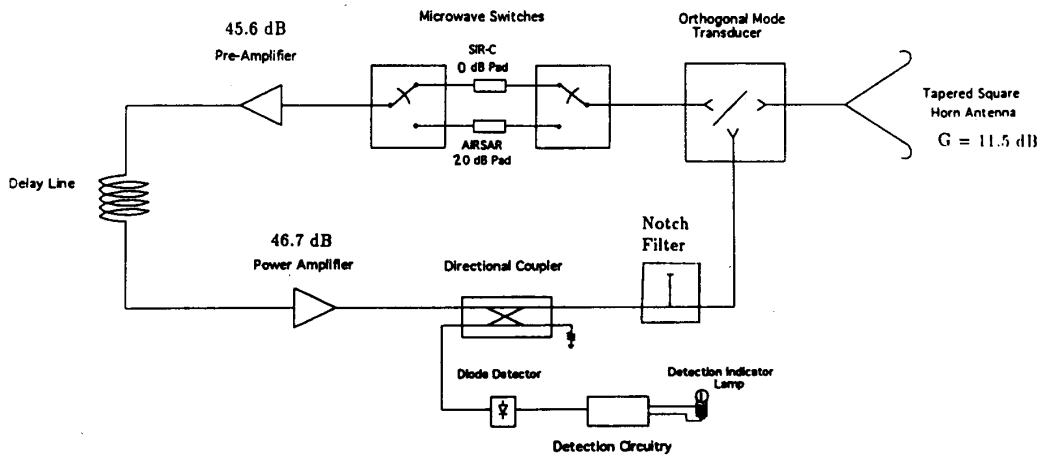

Fig. 3. Simplified block diagram of L-band SAPARC's.

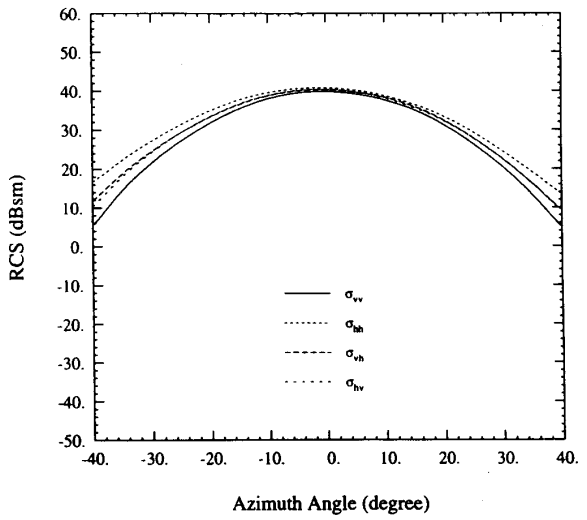

Fig. 4. RCS pattern of an L-band SAPARC.

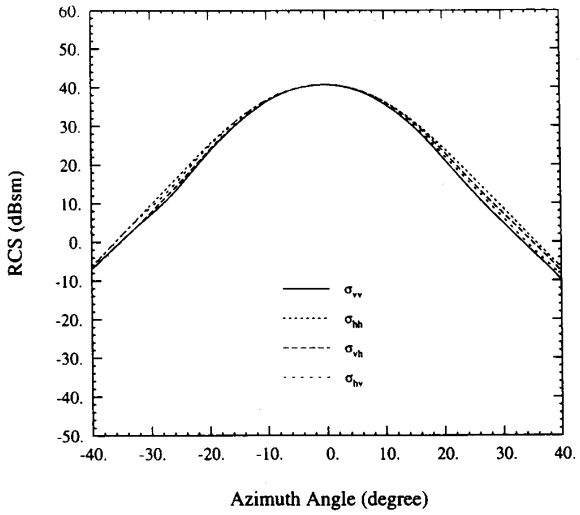

Fig. 5. RCS pattern of a C-band SAPARC.

can then be compared with the RCS-versus-temperature chart of the SAPARC to accurately determine its RCS at the time of the SIR-C overflight.

D. Calibration Algorithms for Polarimetric SAR Systems

We have developed two approaches for calibration of polarimetric synthetic aperture radars. The first approach is based on point calibration targets [6]. In this method the polarimetric ambiguity function of the SAR is estimated from a trihedral in the image. Using an error model similar to the one used in STCT, the calibration constant and distortion parameters of the SAR are obtained. One of the unique features of this technique is that it can account for the possible differences in the ambiguity functions of different polarization channels and thereby effectively remove the cross-talk distortions. Accuracy of this calibration algorithm is directly proportional to the accuracy in the knowledge of the scattering matrix of the trihedral calibration target. The detailed procedure and actual implementation of this technique is given in [6]. This technique and the calibration technique developed by JPL [17] are used as point target calibration algorithms to characterize the radiometric calibration and system distortion of the SIR-C SAR's. Our preliminary results show that the two-point target calibration algorithms provide similar results.

In the second approach a uniform distributed target is used as a calibration target [8]. It is shown that the radar distortion parameters and the radiometric calibration constant can be obtained from a homogeneous distributed target with known differential Mueller matrix. The differential covariance matrix or equivalently the differential Mueller matrix of this target is obtained using the scatterometer systems as described in [7]. For the scatterometer, then, point-target calibration consists of range-gating the response from an elevated sphere to effectively put it in free-space. The antenna pattern, both amplitude and phase, is determined from a careful

lab measurement and remains constant except for a scale factor. The characterized distortion parameters are then used in an algorithm to provide the calibrated differential Mueller matrices of other homogeneous targets in the image. The advantages offered here are as follows: 1) point targets are not needed and the calibration is not influenced by the interaction of the targets with their backgrounds, 2) estimation of the polarimetric ambiguity function is not required, 3) since the differential Mueller matrix is calculated from many independent measurements the effect of noise and measurement errors are minimized.

For an imaging radar it is shown that the measured scattering matrix of a given pixel is given by [6]

$$\mathbf{U}(x,y) = \mathbf{R}\left[\int_A \mathbf{S}^\circ(x',y')\psi(x-x',y-y')\,dx'dy'\right]\mathbf{T} \quad (1)$$

where $\mathbf{R}$ and $\mathbf{T}$ are the receive and transmit distortion matrices, $\psi(x,y)$ is the ambiguity function of the SAR, and $\mathbf{S}^\circ(x,y)$ is the differential scattering matrix of the pixel. In this algorithm it is assumed that the differential scattering matrix of the distributed target is a stationary and ergodic random process. Also assuming that the pixel size is much larger than the field correlation distance and after a long algebraic manipulation it is shown that

$$\langle \mathcal{U}_m \mathcal{U}_n^* \rangle = \omega \sum_{i=1}^{4}\sum_{j=1}^{4} d_{mi} d_{nj}^* \langle \mathcal{S}_i^\circ \mathcal{S}_j^{\circ *} \rangle \quad (2)$$

where $\mathcal{U}_i$ and $\mathcal{S}_j^\circ$ are the elements of the measured and the true differential scattering matrices $(i,j = 1,\ldots,4)$, respectively. In (2), ω is the radiometric calibration constant given by

$$\omega = |R_{vv}T_{vv}|^2 \int_A |\psi(x',y')|^2\,dx'dy'$$

and d_{ij} are the elements of the generalized distortion matrix given by

$$\mathbf{d} = \begin{bmatrix} 1 & x_4 & x_1 & x_1x_4 \\ x_5 & x_6 & x_1x_5 & x_1x_6 \\ x_2 & x_2x_4 & x_3 & x_3x_4 \\ x_2x_5 & x_2x_6 & x_3x_5 & x_3x_6 \end{bmatrix} \quad (3)$$

where

$$x_1 = \frac{R_{vh}}{R_{vv}}, \quad x_2 = \frac{R_{hv}}{R_{vv}}, \quad x_3 = \frac{R_{hh}}{R_{vv}},$$

$$x_4 = \frac{T_{vh}}{T_{vv}}, \quad x_5 = \frac{T_{hv}}{T_{vv}}, \quad x_6 = \frac{T_{hh}}{T_{vv}}.$$

The error model given by (2) provides 16 complex equations; however, since the resulting matrix equation is Hermitian symmetric, there are only six complex plus four real independent equations. The error model is nonlinear, and therefore a search routine (conjugate gradient) is used to find the six complex $(x_1 \cdots x_6)$ and one real (ω) unknowns.

III. Experimental Results

To calibrate radar images acquired by SIR-C and characterize the distortion parameters of the SIR-C SAR's, an array of 8-foot trihedral corner reflectors, PARC's, and SAPARC's were deployed in the Raco Supersite for both the April and the October missions. Only the calibration results of the first SIR-C mission are presented. Raco was chosen as a calibration supersite because it was a cross-over point for the descending and ascending SIR-C tracks. A grass field of more than 50 acres in area was chosen as the homogeneous distributed target. Our choice of distributed targets was limited to only short vegetation with relatively small correlation lengths because of the height limitation of the boom-truck. The grass field was first covered with snow which went through many cycles of melting and freezing during the 13 SIR-C overflights from Apr. 9 to Apr. 18. This physical change gave the target a wide dynamic range in backscattering coefficient as a function of time.

The point calibration targets were boresighted very carefully and their orientation angles were recorded before and after each SIR-C overflight. Polarimetric backscattering measurements at L-, C-, and X-band were conducted immediately after the SIR-C overflight at exactly the same incidence angle $(\pm 0.5^\circ)$. More than 100 independent spatial samples were collected to generate the desired statistics of the backscattered signals. Also the backscattered data were collected over a wide bandwidth (400 MHz) to increase the number of independent samples. Using the bandwidth the number of independent samples is increased by a factor of ten. The collected data were calibrated as outlined in [7] and the differential Mueller matrix of the grass field for each SIR-C pass was acquired. Fig. 6(a)–(c), respectively, show the L-, C-, and X-band backscattering coefficient of the grass field for eleven consecutive SIR-C data-takes starting with data-take 6.1 on Apr. 9. The temporal variation of backscatter as shown in these figures is a result of two factors: 1) the change in incidence angle, and 2) the changes in the target physical status. The incidence angles at which the backscatter measurements were conducted are indicated on the data points of Fig. 6(a)–6(c). The temporal and polarimetric behavior of the backscattering coefficient indicate that the backscatter at L-band was dominated by the scattering from the underlying soil surface, while at C-band and X-band the thatch layer significantly affected the backscatter.

For a complete polarimetric assessment of calibration techniques, the statistical parameters of both the magnitude and the phase of the backscattered signals must be compared. The magnitude information can be directly obtained from the measured Mueller matrix. However, the phase statistics must be computed indirectly from the elements of the Mueller matrix. Assuming that the scattering process is Gaussian, it is shown that the probability density function (PDF) of the phase difference of the scattering matrix elements can be derived from the measured Mueller matrix [18]. It is also shown that the PDF can be fully characterized from two independent parameters. One of these parameters is known as the degree of correlation (α) and the other parameter is known as the coherent phase difference (ξ). The range of variation of α is from 0 to 1 where $\alpha = 0$ corresponds to a uniform distribution and $\alpha = 1$ corresponds to a deterministic phase difference (the PDF is a delta function). The parameter ξ can vary from $-\pi$ to π and indicates the phase difference at which the PDF assumes its maximum.

Fig. 7 shows a typical C-band image of the distributed target calibration site where some of the point targets were

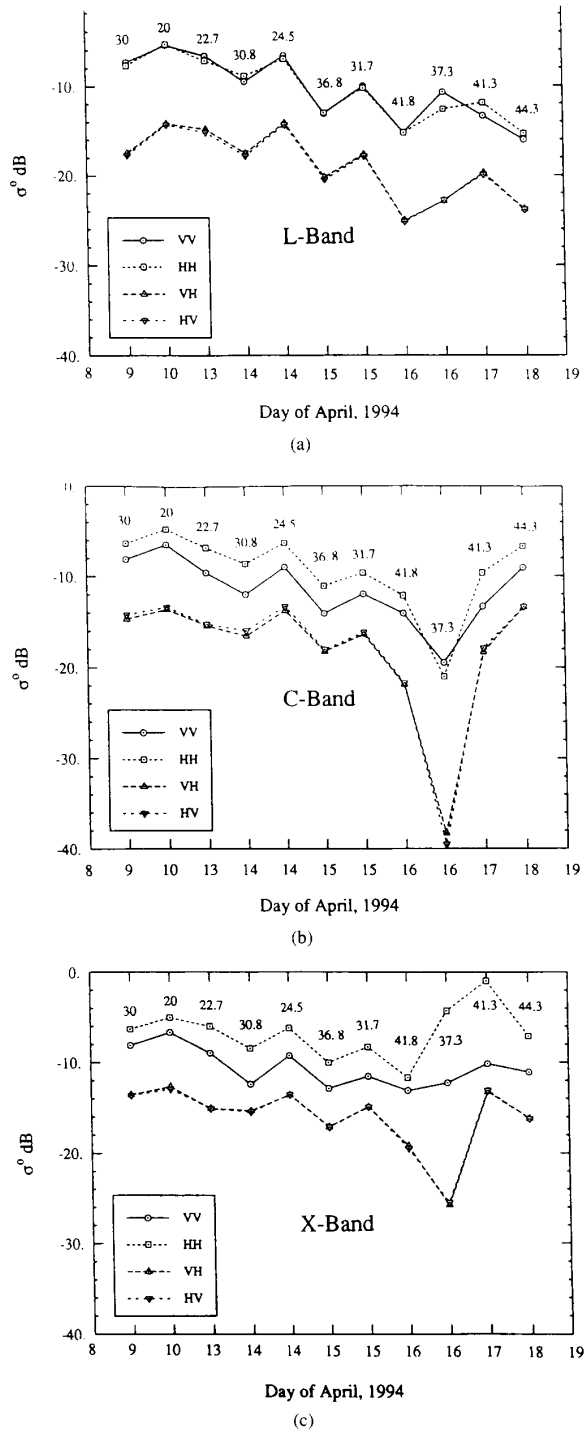

Fig. 6. Backscatter coefficient of the distributed target as a function of time at (a) L-band, (b) C-band, and (c) X-band.

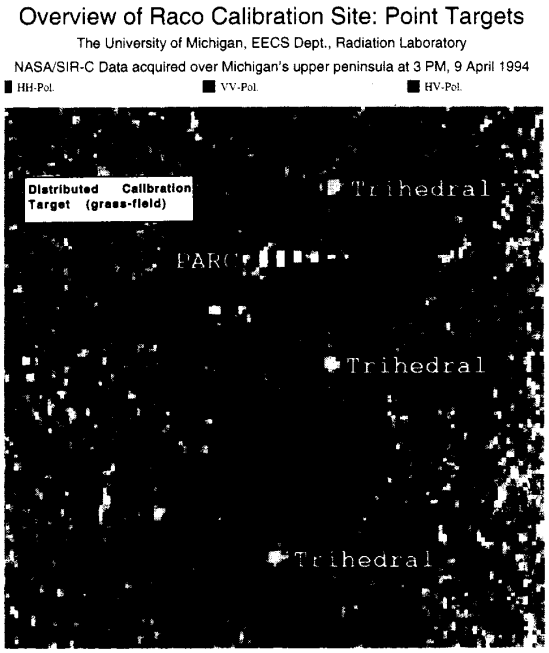

Fig. 7. A typical C-band image of the distributed target (grass-field).

also deployed. The pixels around the point targets were excluded from the calculation of the covariance matrix of the distributed target. Both the point and the distributed target calibration algorithms were used to calibrate the image. The calibration results based on Michigan's [6] and JPL's [17] point calibration algorithms are similar. Therefore only the comparison between Michigan's distributed-target calibration algorithm [8], and the JPL point-target calibration algorithm will be presented. Fig. 8 shows a larger portion of the C-band image where the areas of different land-covers as test distributed targets are indicated. The test distributed targets include: 1) frozen lake, 2) grass-field, 3) shrubs, 4) defoliated deciduous trees, and 5) conifers.

Next we present the comparison of the backscatter coefficients and the parameters of phase difference statistics of the test distributed targets as calibrated by the point and distributed target calibration algorithm. Only the results of the 98.12 (Apr. 15, 1994) and 114.1 (Apr. 16, 1994) data-takes are presented. The distortion parameters of the C-band SAR obtained from the distributed calibration algorithm are summarized in Table I. This table presents the radiometric calibration constant (ω), the cross-talks, and the channel imbalances defined by (3) for the C-band SAR. It should be noted that these parameters are acquired from the single look images. The cross-talk factors (x_1, x_2, x_4, x_5) are all small quantities as expected and the variabilities in the cross-talk factors between the two data-takes resulted from minimizing the difference between the truck and SAR backscatter measurements. Also the channel imbalances (x_3, x_6) are close to unity (0 dB) as expected. The overall system channel imbalances $(R_{hh}T_{hh}/(R_{vv}T_{vv}))$ for data-takes 98.12 and 114.1 are $1.53\angle -23$ and $1.43\angle 19.5$ respectively. This system change might have been caused by changes in the antenna elements controlling the incidence angle (antenna beam is steered electronically). Fig. 9 compares the backscattering coefficients $(\sigma^\circ_{vv}, \sigma^\circ_{hh}, \sigma^\circ_{vh})$ of all the test distributed targets for the 98.12 and 114.1 C-band images

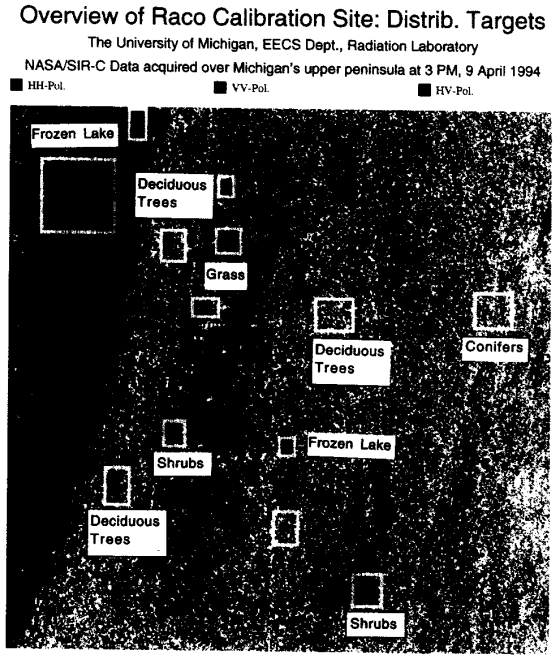

Fig. 8. A typical C-band image showing different test targets.

TABLE I
THE DISTORTION PARAMETERS OF THE SIR-C C-BAND SAR (MAGNITUDES ARE EXPRESSED IN dB)

Data-Take No.	ω	$x_1 = \frac{R_{vh}}{R_{vv}}$	$x_2 = \frac{R_{hv}}{R_{vv}}$	$x_3 = \frac{R_{hh}}{R_{vv}}$
98.12	7.12	$-29.7\angle 97°$	$-28.2\angle -105°$	$0.85\angle -99°$
114.1	6.99	$-23.7\angle 89°$	$-26.2\angle 6.5°$	$-0.38\angle -77°$

Data-Take No.	$x_4 = \frac{T_{vh}}{T_{vv}}$	$x_5 = \frac{T_{hv}}{T_{vv}}$	$x_6 = \frac{T_{hh}}{T_{vv}}$
98.12	$-27.3\angle -16°$	$-18\angle -107°$	$0.68\angle 76.15°$
114.1	$-24.3\angle 12°$	$-26.6\angle 16°$	$1.8\angle 96.5°$

when calibrated by point and distributed target calibration algorithms. It is shown that the maximum discrepancy between the two methods is about 2 dB. The discrepancies for data-takes 98.12 and 114.1 are due to the differences in estimation of the channel imbalance and radiometric calibration constant respectively. These discrepancies can be the direct result of the uncertainties in the RCS of point targets used in the point-target calibration procedure. One example of such uncertainties can be found in [19] where the C-band RCS varied by as much as 4 dBm^2 due to wind-induced deformations. Similar comparisons are shown in Figs. 10 and 11 for the parameters of the phase difference statistics. Fig. 10 shows the comparison for the degree of correlation of both the co- and cross-polarized phase differences for data-takes 6.1 and 114.1. The agreement is excellent except for α_x of the ice covered lake on Apr. 9 (data-take 6.1). For most natural targets with azimuthal symmetry the co- and cross-polarized components of the scattering matrix are uncorrelated which renders $\alpha_x = 0$. This is an inherent assumption in the JPL calibration algorithm which may not be valid for some targets such as sea ice. The comparison of the copolarized phase difference is shown in

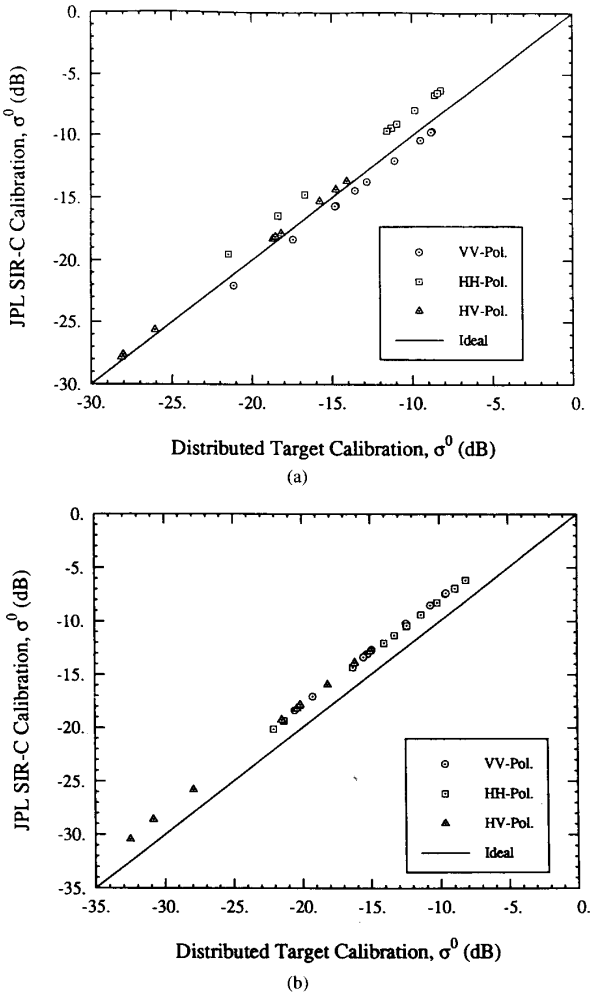

Fig. 9. Comparison of the measured backscattering coefficients of all the test distributed targets; (a) 98.12 data-take and (b) 114.1 data-take.

Fig. 11 where a constant discrepancy of about 10° is observed. This discrepancy can again be attributed to the uncertainties in the scattering matrix of the point calibration targets.

Examination of different point targets in the image may reveal the uncertainties in their RCS. Figure 12a gives the total integrated power of three trihedrals in the distributed target calibration site showing that there is a 2.5 dB difference between two of the 8-feet trihedrals. Figure 13b compares the normalized RCS of the C-band SAPARC (oriented at 45°) acquired from the two calibrated images. It is expected that power in different polarization channels be the same for this PARC; however, due to possible errors in target orientation and its interaction with the ground there is about 2 dB variations from the expected result. Similar results were obtained for other C-band images.

IV. CONCLUSION

In this paper, the required procedures for external calibration of polarimetric SAR's onboard the Shuttle (SIR-C) were sum-

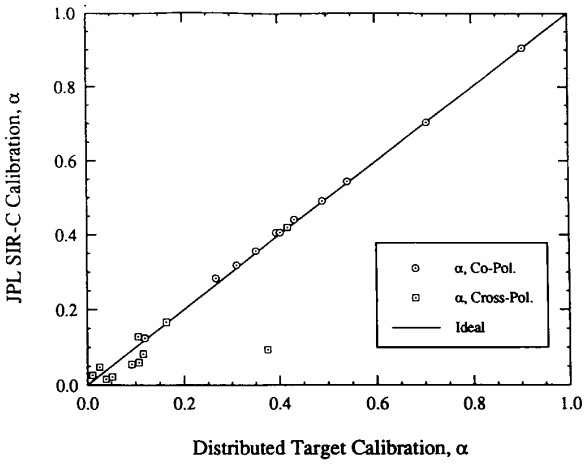

(a)

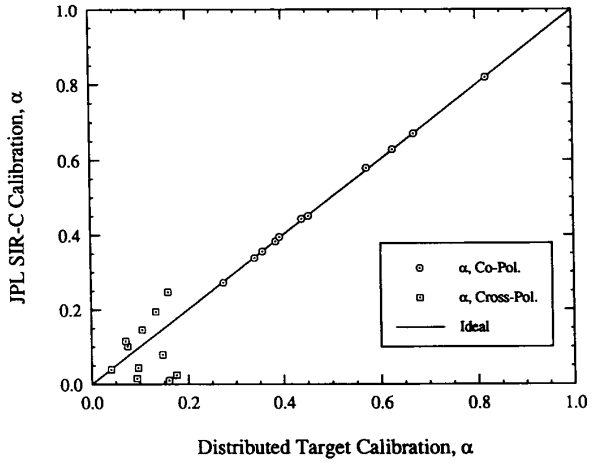

(b)

Fig. 10. Comparison of the measured degree of correlation for all the test distributed targets at C-band; (a) 6.1 data-take (b) 114.1 data-take.

marized. Some preliminary results based on C-band images of the first SIR-C mission were presented. Two calibration algorithms, one based on point calibration targets and the other based on a known distributed target were used to calibrate the images. Trihedral corner reflectors and active radar calibrators were used as point calibration targets. A grass-field was used as the homogeneous distributed target and its radar response was characterized using the University of Michigan polarimetric scatterometer systems. Comparing the covariance matrices of the distributed target as measured by the scatterometers and SIR-C, the radar distortion parameters and the radiometric calibration constant were obtained. The polarimetric responses of five different types of distributed targets acquired from images calibrated by the point and distributed calibration algorithms were compared. A maximum discrepancy of about 2 dB in backscattering coefficients were observed between the two calibration methods. Also a maximum discrepancy of about 10° was observed between the coherent phase differences. In general very good agreement was obtained for the degree of

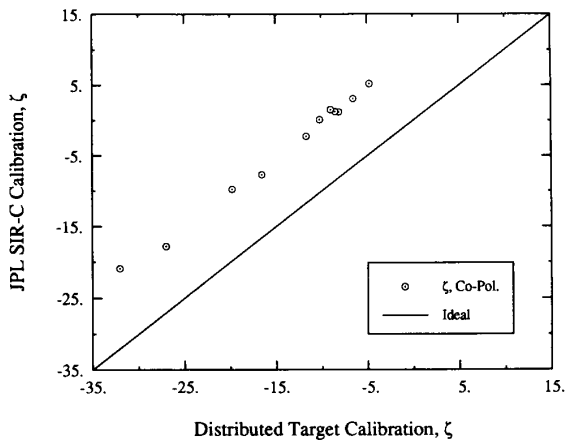

Fig. 11. Comparison of the measured copolarized phase difference for all the test distributed targets at C-band (114.1 data-take).

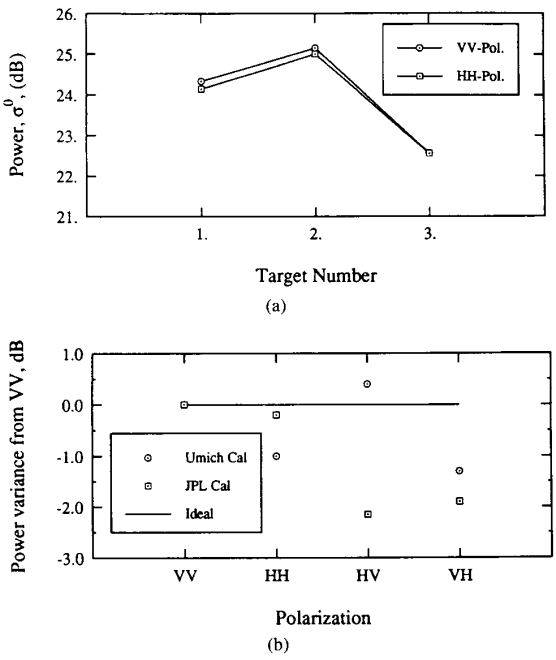

(a)

(b)

Fig. 12. The variability of the point targets: (a) integrated power for three 8-foot trihedrals at C-band, and (b) Polarization response of the C-band SAPARC after calibration.

correlation. The variability of the radar responses of point targets in the radar images suggest that the discrepancies between the two calibration methods are caused by the uncertainties in the RCS of point calibration targets. The calibration algorithm based on a distributed target is believed to be as accurate as the scatterometer measurements of distributed targets (±0.5 dB in magnitude and ±5° in phase).

REFERENCES

[1] J. J. van Zyl, "Calibration of polarimetric radar images using only image parameters and trihedral corner reflector responses," *IEEE Trans. Geosci. Remote Sensing*, vol. 28, p. 337, May 1990.

[2] J. D. Klein and A. Freeman, "Quandpolarization SAR calibration using target reciprocity," *J. Electromag. Waves Appl.*, vol. 5, no. 7, p. 735, 1991.
[3] A. Freeman, Y. Chen, and C. L. Werner, "Polarimetric SAR calibration experiment using active radar calibrators," *IEEE Trans. Geosci. Remote Sensing*, vol. 28, no. 2, p. 224, Mar. 1990.
[4] A. Freeman, "SAR calibration: An Overview," *IEEE Trans. Geosci. Remote Sensing*, vol. 30, no. 6, p. 1107, Nov. 1992.
[5] A. L. Gray, P. W. Vachon, C. E. Livingstone, and T. I. Lukowski, "Synthetic aperture radar calibration using reference reflectors," *IEEE Trans. Geosci. Remote Sensing*, vol. 28, p. 374, May 1990.
[6] K. Sarabandi, L. E. Pierce, and F. T. Ulaby, "Calibration of a polarimetric imaging SAR," *IEEE Trans. Geosci. Remote Sensing*, vol. 30, p. 540, May 1992.
[7] K. Sarabandi, Y. Oh and F. T. Ulaby, "Measurement and calibration of differential Mueller matrix of distributed targets," *IEEE Trans. Antennas Propagat.*, vol. 40, pp. 1524–1532, Dec. 1992.
[8] K. Sarabandi, "Calibration of a polarimetric synthetic aperture radar using a known distributed target," *IEEE Trans. Geosci. Remote Sensing*, vol. 32, pp. 575–583, May 1994.
[9] K. Sarabandi, L. E. Pierce, Y. Oh, M. C. Dobson, A. Freeman, and P. Dubois, "Cross calibration experiment using JPL AIRSAR and truck-mounted polarimetric scatterometers," *IEEE Trans. Geosci. Remote Sensing*, vol. 32, no. 5, Sept. 1994.
[10] K. Sarabandi, F. T. Ulaby and M. A. Tassoudji, "Calibration of polarimetric radar systems with good polarization isolation," *IEEE Trans. Geosci. Remote Sensing*, vol. 28, no. 1, Jan. 1990.
[11] M. W. Whitt, F. T. Ulaby, P. Polatin and V. V. Liepa, "A general polarimetric radar calibration technique: Theory and experiment," *IEEE Trans. Antennas Propagat.*, vol. 39, no. 1, Jan. 1991.
[12] K. Sarabandi and F. T. Ulaby, "A convenient technique for polarimetric calibration of radar systems," *IEEE Trans. Geosci. Remote Sensing*, vol. 28, Nov. 1990.
[13] D. R. Brunfeldt and F. T. Ulaby, "Active calibrators for radar calibration," *IEEE Trans. Geosci. Remote Sensing*, vol. 22, Mar. 1984.
[14] D. Kahny and J. J. van Zyl, "How does corner reflector construction affect polarimetric SAR calibration?," *IGARSS '90*, 1990, vol. 2, p. 1093.
[15] K. Sarabandi and Y. Oh, "RCS measurement of polarimetric active radar calibrators," Univ. Michigan, Ann Arbor, Radiation Lab. Rep. No. 027165-1-T, June 1990.
[16] K. Sarabandi, Y. Oh, and F. T. Ulaby, "Application and performance characterization of polarimetric active radar calibrator," *IEEE Trans. Antennas Propagat.*, vol. 40, Oct. 1992.
[17] J. J. van Zyl, C. F. Burnette, H. A. Zebker, A. Freeman, and J. Holt, *POLCAL User's Manual*. Pasadena, CA: Jet Propulsion Laboratory, Aug. 1990.
[18] K. Sarabandi, "Derivation of phase statistics of distributed targets from the Mueller matrix," *Radio Sci.*, vol. 27, no. 5, pp. 553–560, 1992.
[19] van den Broek and J. S. Groot, "Intercalibration of satellite and airborne SAR: A comparitive study of ERS-1 and AirSAR/PHARS SAR Data," *Can. J. Remote Sensing*, vol. 19, pp. 209–217, Aug. 1993.

Kamal Sarabandi (M'90–SM'92), for a photograph and biography, see p. 857 of this issue.

Leland E. Pierce (S'85–M'85), received the B.S. degrees in both electrical and aerospace engineering and the M.S. and Ph.D. degrees in electrical engineering from the University of Michigan, Ann Arbor, in 1983, 1986, and 1991, respectively.

Since 1991, he has been the head of the Microwave Image Processing Facility within the Radiation Laboratory in the Electrical Engineering and Computer Science Department, University of Michigan, where he is responsible for research into the uses of Polarimetric SAR systems for remote sensing applications, specifically forest canopy parameter inversion.

M. Craig Dobson, photograph and biography not available at the time of publication.

Fawwaz T. Ulaby (M'68–SM'74–F'80), received the B.S. degree in physics from American University of Beirut, Beirut, Lebanon, and the M.S.E.E. and Ph.D. degrees in electrical engineering from the University of Texas, Austin, in 1964, 1966, and 1968, respectively.

He is R. Jamison and Betty Williams Professor of Electrical Engineering and Computer Science at the University of Michigan, Ann Arbor and the Director of the NASA Center for Space Terahertz Technology. His current interests include microwave and millimeter wave remote sensing, radar systems, and radio wave propagation. He has authored eight books and more than 400 papers and reports on these subjects.

Dr. Ulaby has received the Eta Kappa Nu Association C. Holmes MacDonald Award in 1975, the IEEE Geoscience and Remote Sensing Distinguished Achievement Award in 1983, the IEEE Centennial Medal in 1984, the American Society of Photogrammetry's Presidential Citation for Meritorious Science in 1984, the Kuwait Prize in applied science in 1986, the NASA Group Achievement Award in 1990, and the University of Michigan Distinguished Faculty Achievement Award in 1991. He has served as President of the IEEE Geoscience and Remote Sensing Society (1980–1982), as Executive Editor of its Transactions (1983–1985), and as General Chairman of several international symposia. He is a member of URSI Commission F, the National Academy of Engineering, and serves on several scientific boards and professional committees.

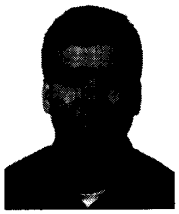

James M. Stiles was born in Kansas City, MO, in 1961. He received the B.S.E.E. degree from the University of Missouri, Columbia, and the M.S.E.E. degree from Southern Methodist University, Dallas, TX, in 1983 and 1987, respectively. He is pursuing the Ph.D. degree in electrical engineering at the University of Michigan, Ann Arbor.

From 1983 to 1990, he was an RF design engineer for Texas Instruments Inc., Dallas, TX. His research interests include electromagnetic scattering from vegetation, and application of estimation theory to microwave remote sensing.

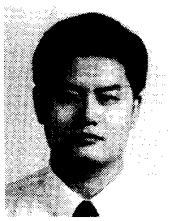

T. C. Chiu was born November 3, 1968, in Kaohsiung, Taiwan. He received the B.S. and M.S. degrees in electrical engineering from National Taiwan University, Taipei, Taiwan, in 1990 and 1992, respectively. He is pursuing the Ph.D. degree in electrical engineering at the University of Michigan, Ann Arbor.

He is a Research Assistant with the Radiation Laboratory, University of Michigan. His research interests include microwav remote sensing and calibration of radar systems.

R. De Roo, photograph and biography not available at the time of publication.

R. Hartikka, photograph and biography not available at the time of publication.

A. Zambetti, photograph and biography not available at the time of publication.

Anthony Freeman (M'83–SM'94), for photograph and biography, please see p. 114 of the January issue of this TRANSACTIONS.